

First-Principles Study of the Honeycomb-Lattice Iridates Na_2IrO_3 in the Presence of Strong Spin-Orbit Interaction and Electron Correlations

Youhei Yamaji, Yusuke Nomura, Moyuru Kurita, Ryotaro Arita and Masatoshi Imada
 Department of Applied Physics, University of Tokyo, Hongo, Bunkyo-ku, Tokyo, 113-8656, Japan.
 (Dated: September 10, 2018)

An effective low-energy Hamiltonian of itinerant electrons for iridium oxide Na_2IrO_3 is derived by an *ab initio* downfolding scheme. The model is then reduced to an effective spin model on a honeycomb lattice by the strong coupling expansion. Here we show that the *ab initio* model contains spin-spin anisotropic exchange terms in addition to the extensively studied Kitaev and Heisenberg exchange interactions, and allows to describe the experimentally observed zigzag magnetic order, interpreted as the state stabilized by the antiferromagnetic coupling of the ferromagnetic chains. We clarify possible routes to realize quantum spin liquids from existing Na_2IrO_3 .

Introduction.— Cooperation and competition between strong electron correlations and spin-orbit couplings have recently attracted much attention. Iridium oxides offer playgrounds for such an interplay and indeed exhibit intriguing rich phenomena [1–4].

Especially, a theoretical prediction [1, 2] on the possible realization of quantum spin liquid state and Majorana fermion state proven by Kitaev [5] as the ground state of an exactly solvable model now called Kitaev model has inspired extensive studies on A_2IrO_3 ($\text{A} = \text{Na}$ or Li) as a model system to realize the Kitaev spin liquid. However, although Na_2IrO_3 is an insulator (presumably Mott insulator) with the optical gap ~ 0.35 eV [6], it was shown that Na_2IrO_3 does not show spin liquid properties experimentally but exhibits a zigzag type magnetic order [7, 8].

The Kitaev-Heisenberg model on the honeycomb lattice [1, 2, 9–11] was further proposed to describe Na_2IrO_3 , which includes isotropic superexchange couplings in addition to the Kitaev-type anisotropic nearest-neighbor Ising interactions whose anisotropy axes depend on the bond directions. However, it turned out that this model cannot be straightforwardly consistent with the zigzag order either. This discrepancy inspired further studies on suitable low-energy effective hamiltonians for A_2IrO_3 with $\text{A} = \text{Na}$ or Li . First, models with further neighbor couplings [7, 8, 12, 13] were studied. Additional Ising anisotropy [14] due to a strong trigonal distortion, which actually contradicts the distortions in the experiments [8] and in the *ab initio* treatments, was also examined. Quasimolecular orbitals [15], instead of the atomic orbitals assumed in the Kitaev-Heisenberg model were claimed as a proper choice of the starting point. So far the origin of the zigzag type antiferromagnetic order observed for Na_2IrO_3 and the possible route to realize the quantum spin liquid are controversial.

In this Letter, we derive an *ab initio* spin model for Na_2IrO_3 and show that trigonal distortions present in Na_2IrO_3 in addition to the spin-orbit couplings hold the key: The simplest and realistic spin model for A_2IrO_3 will turn out to modify the Kitaev-Heisenberg hamiltonian by

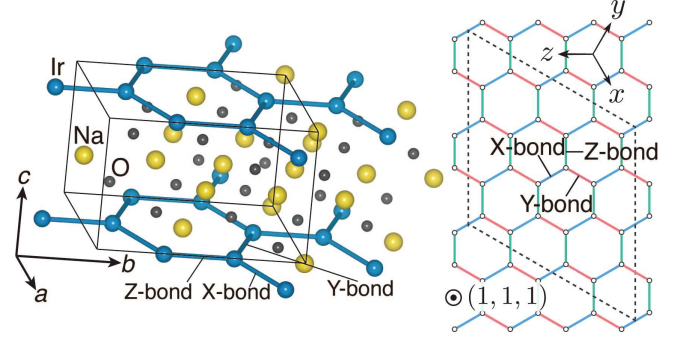


FIG. 1: (color online): Left panel: Crystal structure of Na_2IrO_3 . Right panel: Honeycomb lattice with X-, Y-, and Z-bonds. Same colored bonds indicate the same group. The x , y , and z axes in defining the t_{2g} -orbitals are illustrated as directions out of the honeycomb plane. The honeycomb plane is then perpendicular to $(x, y, z) = (1, 1, 1)$. The dashed boundary represents a 24-site cluster used later for the exact diagonalization.

additional anisotropic couplings as

$$\hat{H} = \sum_{\Gamma=X,Y,Z} \sum_{\langle \ell, m \rangle \in \Gamma} \vec{\hat{S}}_{\ell}^T \mathcal{J}_{\Gamma} \vec{\hat{S}}_m, \quad (1)$$

where $\vec{\hat{S}}_{\ell}^T = (\hat{S}_{\ell}^x, \hat{S}_{\ell}^y, \hat{S}_{\ell}^z)$ is a vector of SU(2) spin operators. The exchange couplings are given in matrices \mathcal{J}_{Γ} . The summations are over the nearest-neighbor pairs $\langle \ell, m \rangle$. The group of bond Γ with $\Gamma = X, Y$ and Z is defined in Fig. 1. The exchange matrices are parametrized as

$$\mathcal{J}_Z = \begin{bmatrix} J & I_1 & I_2 \\ I_1 & J & I_2 \\ I_2 & I_2 & K \end{bmatrix}, \mathcal{J}_X = \begin{bmatrix} K' & I_2'' & I_2' \\ I_2'' & J'' & I_1' \\ I_2' & I_1' & J' \end{bmatrix}, \quad (2)$$

$$\mathcal{J}_Y = \begin{bmatrix} J'' & I_2'' & I_1' \\ I_2'' & K' & I_2' \\ I_1' & I_2' & J' \end{bmatrix},$$

where we choose a real and symmetric parameterization by using U(1)- and SU(2)-symmetry of electron wave functions and spin operators, respectively. The details

of these exchange parameters are described in the following discussion.

In addition to the Kitaev coupling K and K' , and XY-type exchange J , magnetic anisotropy induced by a combination of spin-orbit couplings and trigonal distortions appears as anisotropic couplings such as I_1 and I_2 . Here we note that our parameterization of the Kitaev term is different from that of Refs.1, 2, 11: The Kitaev term K in the present Letter corresponds to $-|K| + J$ in Refs.1, 2, 11. These anisotropic couplings drastically change candidate quantum phases and competition among them in Na_2IrO_3 and related materials. With these extensions, we show that the model allows a realistic description of Na_2IrO_3 and provides a basis for further search of quantum spin liquids. To achieve quantitative accuracy, we include the further neighbor couplings in our numerical calculations as detailed later.

Ab initio derivation and estimate of itinerant effective hamiltonian.— To discuss low-energy physics of Na_2IrO_3 , we employ a recently proposed multi-scale *ab initio* scheme for correlated electrons (MACE) [16]: First, we obtain the global band structure using the density functional theory (DFT). Second, using a Wannier projection on the Ir $5d$ t_{2g} target bands, we derive an effective model for the Ir $5d$ t_{2g} orbitals by the downfolding procedure taking into account the renormalization from the states other than the Ir $5d$ t_{2g} orbitals.

The global electronic structure was obtained by performing the density functional calculations using the Elk full-potential linearized augmented plane-wave code [17] with the Perdew-Wang exchange-correlation functional [18]. The resultant electronic structures agree with the previous DFT results [15] (see Appendix A).

We next constructed the Wannier orbitals from the Ir t_{2g} bands following the same procedure described in Ref. [19]. One body parameters $t_{\ell,m;a,b}^{\sigma,\sigma'}$ in the low-energy hamiltonian are given by the matrix elements of the Wannier orbitals as

$$t_{\ell,m;a,b}^{\sigma,\sigma'} = \int d\mathbf{r}_1 d\mathbf{r}_2 w_{\ell a \sigma}^*(\mathbf{r}_1) \hat{H}_{\text{KS}} w_{m b \sigma'}(\mathbf{r}_2) \quad (3)$$

with the Kohn-Sham hamiltonian \hat{H}_{KS} and the indices for sites ℓ and m , orbitals a and b , and spins σ and σ' .

The effective Coulomb interactions between these orbitals are estimated by the constrained random phase approximation (cRPA) [20]. Using the density response code for Elk [21], we obtain the *constrained* susceptibility of the noninteracting Kohn-Sham electrons $\chi_0(\mathbf{r}, \mathbf{r}', \omega)$ where contribution of particle-hole excitations within the target t_{2g} bands is excluded. We then calculate the partially-screened Coulomb interaction

$$W(\mathbf{r}, \mathbf{r}', \omega) = \frac{1}{|\mathbf{r} - \mathbf{r}'|} + \int d\mathbf{r}_1 d\mathbf{r}_2 \frac{\chi_0(\mathbf{r}_1, \mathbf{r}_2, \omega)}{|\mathbf{r} - \mathbf{r}_1|} W(\mathbf{r}_2, \mathbf{r}', \omega),$$

which yields the Coulomb interaction between the Wan-

nier orbitals w as

$$U_{\mathcal{K}\mathcal{L}\mathcal{M}\mathcal{N}} = \lim_{\omega \rightarrow 0} \int d\mathbf{r}_1 d\mathbf{r}_2 w_{\mathcal{K}}^*(\mathbf{r}_1) w_{\mathcal{L}}^*(\mathbf{r}_2) W(\mathbf{r}_1, \mathbf{r}_2, \omega) \times w_{\mathcal{M}}(\mathbf{r}_1) w_{\mathcal{N}}(\mathbf{r}_2),$$

where $\mathcal{K}, \mathcal{L}, \mathcal{M}$, and \mathcal{N} are the combined indices for orbital and site.

Ab initio model for t_{2g} hamiltonian— The derived multiband model consisting of t_{2g} -manifold of the iridium atoms is given by the t_{2g} -hamiltonian

$$\hat{H}_{t_{2g}} = \hat{H}_0 + \hat{H}_{\text{tri}} + \hat{H}_{\text{SOC}} + \hat{H}_U, \quad (4)$$

where each decomposed part is determined in the following: The hopping terms are given by

$$\hat{H}_0 = \sum_{\ell \neq m} \sum_{a,b=xy,yz,zx} \sum_{\sigma,\sigma'} t_{\ell,m;a,b}^{\sigma,\sigma'} \left[\hat{c}_{\ell a \sigma}^\dagger \hat{c}_{m b \sigma'} + \text{h.c.} \right]. \quad (5)$$

Here we note that, among all the hoppings, the dominant terms are the nearest-neighbor hoppings $t \simeq t_{\ell,m;a,b}^{\sigma,\sigma} \simeq t_{\ell,m;b,a}^{\sigma,\sigma}$ that satisfy $(a,b) = (zx, xy)$, (xy, yz) , or (yz, zx) with $(\ell, m) \in X, Y$, and Z , which is consistent with the original proposal [1] for the Kitaev couplings. The x -, y -, and z -axes are illustrated in Fig. 1.

The onsite atomic part is derived from Eq. (3) with $\ell = m$ and can be described as the contribution from the trigonal distortion (with orbital-dependent chemical potentials) and the atomic part of the spin-orbit coupling by introducing a vector representation $\vec{\hat{c}}_\ell^\dagger = (\hat{c}_{\ell yz\uparrow}^\dagger, \hat{c}_{\ell yz\downarrow}^\dagger, \hat{c}_{\ell zx\uparrow}^\dagger, \hat{c}_{\ell zx\downarrow}^\dagger, \hat{c}_{\ell xy\uparrow}^\dagger, \hat{c}_{\ell xy\downarrow}^\dagger)$ as

$$\hat{H}_{\text{tri}} = \sum_{\ell} \vec{\hat{c}}_\ell^\dagger \begin{bmatrix} -\mu_{yz} & \Delta & \Delta \\ \Delta & -\mu_{zx} & \Delta \\ \Delta & \Delta & -\mu_{xy} \end{bmatrix} \hat{\sigma}_0 \vec{\hat{c}}_\ell, \quad (6)$$

and

$$\hat{H}_{\text{SOC}} = \frac{\zeta_{\text{so}}}{2} \sum_{\ell} \vec{\hat{c}}_\ell^\dagger \begin{bmatrix} 0 & +i\hat{\sigma}_z & -i\hat{\sigma}_y \\ -i\hat{\sigma}_z & 0 & +i\hat{\sigma}_x \\ +i\hat{\sigma}_y & -i\hat{\sigma}_x & 0 \end{bmatrix} \vec{\hat{c}}_\ell. \quad (7)$$

Both the off-diagonal elements of the spin-independent part \hat{H}_{tri} and the spin-dependent part \hat{H}_{SOC} can be well described by a single parameter Δ and ζ_{so} , respectively. Due to the inherent crystal anisotropy differentiating Ir-Ir bonds along the b -axis from others [22], the chemical potential for the xy -orbitals, μ_{xy} , is different from μ_{yz} and μ_{zx} . The symmetry of these terms is slightly broken in the real crystal due to the stacking fault along the c -axis and the locations of other ions. However the deviation is much smaller than 0.005 eV.

The Coulomb term expressed by the Wannier orbital basis is well described by a symmetric form as

$$\hat{H}_U = U \sum_{\ell} \sum_{a=yz,zx,xy} \hat{n}_{\ell a \uparrow} \hat{n}_{\ell a \downarrow} + \sum_{\ell \neq m} \sum_{a,b} \frac{V_{\ell,m}}{2} \hat{n}_{\ell a} \hat{n}_{m b}$$

one-body (eV)	t	$\mu_{xy} - \mu_{yz, zx}$	ζ_{so}	Δ
	0.27	0.035	0.39	-0.028
two-body (eV)	U	U'	J_H	V
	2.72	2.09	0.23	1.1

TABLE I: One-body and two-body parameters for \hat{H}_{t2g} . The most relevant hopping parameter t , the atomic spin-orbit coupling ζ , and the trigonal distortion Δ , are shown for one-body part. Here, t is for $t_{\ell, m; \xi, \eta}^{\sigma, \sigma'}$ for $\langle \ell, m \rangle$ being the Z bond and its symmetric replacement for X and Y bonds. As for the two-body parameters, we list the cRPA results for the local intra-orbital Coulomb repulsion U , the Hund's rule coupling J_H , and the orbital-independent nearest-neighbor Coulomb repulsion V . Other small one-body parameters are given in Appendix D.

\mathcal{J}_Z (meV)	K	J	I_1	I_2		
	-30.7	4.4	-0.4	1.1		
$\mathcal{J}_{X,Y}$ (meV)	K'	J'	J''	I'_1	I'_2	I''_2
	-23.9	2.0	3.2	1.8	-8.4	-3.1

TABLE II: Nearest-neighbor exchange couplings derived by the strong coupling expansion from the *ab initio* t_{2g} model.

$$\begin{aligned}
& + \sum_{\ell} \sum_{a < b} \sum_{\sigma} [U' \hat{n}_{\ell a \sigma} \hat{n}_{\ell b \bar{\sigma}} + (U' - J_H) \hat{n}_{\ell a \sigma} \hat{n}_{\ell b \sigma}] \\
& + J_H \sum_{\ell} \sum_{a \neq b} \left[\hat{c}_{\ell a \uparrow}^{\dagger} \hat{c}_{\ell b \downarrow}^{\dagger} \hat{c}_{\ell a \downarrow} \hat{c}_{\ell b \uparrow} + \hat{c}_{\ell a \uparrow}^{\dagger} \hat{c}_{\ell a \downarrow}^{\dagger} \hat{c}_{\ell b \downarrow} \hat{c}_{\ell b \uparrow} \right], \quad (8)
\end{aligned}$$

with the local intra-orbital Coulomb repulsion, U , inter-orbital Coulomb repulsion, U' , the Hund's rule coupling, J_H , the inter-atomic Coulomb repulsion, $V_{\ell, m}$, and $\hat{n}_{\ell a} = \hat{n}_{\ell a \uparrow} + \hat{n}_{\ell a \downarrow}$. The orbital dependences of U , J_H and V are negligibly small.

The obtained tight binding parameters are given in Table I. We also list the orbital-averaged values of U , U' , J_H and V obtained by the cRPA. We note that $\Delta = -28$ meV for the t_{2g} model [23]. One might think that $\Delta = -28$ meV looks a tiny parameter. However it is crucial to keep it because it generates relevant anisotropy illustrated later in Fig. 3.

Strong coupling limit, Minimal spin model for A_2IrO_3 .— The *ab initio* parameters for the generalized Kitaev-Heisenberg model (1) are derived from t_{2g} hamiltonian \hat{H}_{t2g} in Eq.(4) by the second order perturbation theory: Here we take $\hat{H}_{tri} + \hat{H}_{SOC} + \hat{H}_U$ as an unperturbed hamiltonian and \hat{H}_0 as a perturbation. Since the ground state of $\hat{H}_{tri} + \hat{H}_{SOC} + \hat{H}_U$ is degenerate, we employ the standard degenerate perturbation theory. If we neglect Δ and μ_a ($a = yz, zx, xy$), the lowest Kramers doublets become so-called $J_{eff}=1/2$ states. The atomic ground state of an isolated iridium atom is preserved to be doublet irrespective of the amplitudes of Δ (see Appendix B),

whose degeneracy is protected by the time-reversal symmetry. Then the generalized Kitaev-Heisenberg model describing pseudospin degrees of freedom is justified as an effective model in the ground state as well as at a finite temperature unless it exceeds both of Δ and ζ_{so} .

The exchange couplings \mathcal{J}_Z , \mathcal{J}_X , \mathcal{J}_Y , and further neighbor couplings are derived through the second order perturbation theory by numerically diagonalizing the local part of the hamiltonian $\hat{H}_{tri} + \hat{H}_{SOC} + \hat{H}_U$ and by including all order terms with respect to ζ_{so} and Δ , irrespective of their amplitudes. (See Appendix C, D, and E.) Thus obtained *ab initio* values for Na_2IrO_3 are given in Table II. We remark that $K \sim -30.1$ meV is negative and $J \sim 4.4$ meV is positive for the Z -bonds. For numerical calculations, we also include the 2nd and 3rd neighbor couplings for more accurate *ab initio* calculations (see Appendix D).

The model (1) with the *ab initio* parameters in Table II together with small and detailed 2nd and 3rd exchange couplings (see Table III in Appendix D) was solved by the exact diagonalization for a 24-site cluster. We also calculate finite temperature properties for the cluster by using the thermal pure quantum states [24], which offers an algorithm similar to the finite-temperature Lanczos [25] and earlier works [26]. They well reproduce the experimentally observed zigzag magnetic order as the ground state and finite temperature properties. See detailed results in later discussions for Fig.2.

Neither large further neighbor exchange couplings [7, 8, 12, 13] nor antiferromagnetic Kitaev couplings $K > 0$ [11, 27] assumed and required to reproduce the experimental zigzag magnetic order in the literature are realistic in the *ab initio* point of view. In addition, the amplitudes of the anisotropic couplings I_1 and I_2 comparable with J are crucially important to reproduce the experimental results, contrary to the assumptions in Refs. 11 and 27. The e_g -orbital degrees of freedom, proposed to change the sign of K in Ref.11 and neglected in the present Letter, generate only minor corrections (see Appendix F).

The stabilization of the zigzag order is interpreted as follows: If we assume the magnetic ordered moment along $(x, y, z) = (1, 1, 0)$, the zigzag order is interpreted as ferromagnetically-ordered chains consisting of the X - and Y -bonds (stabilized by K' and I'_2), antiferromagnetically coupled to each other by the Z -bonds with J , which is in contrast to a quantum-chemistry estimate that neglects I_2 , I'_2 , and I''_2 [22]. Indeed, these four exchange couplings, $K \sim K' < 0$, $J > 0$, and $I''_2 < 0$, are crucial to reproduce the zigzag order (see Appendix G). The alignment along $(1, 1, 0)$ assumed here indeed agrees with the result of the pinning field analysis (see Appendix H) shown in Fig.2(a). It is also confirmed by the nearest-neighbor spin-spin correlations, $\langle \hat{S}_{\ell}^x \hat{S}_m^x \rangle = \langle \hat{S}_{\ell}^y \hat{S}_m^y \rangle = -0.021$, $\langle \hat{S}_{\ell}^z \hat{S}_m^z \rangle = 0.128$, for Z -bond, and $\langle \hat{S}_{\ell}^x \hat{S}_m^x \rangle = 0.052(0.098)$, $\langle \hat{S}_{\ell}^y \hat{S}_m^y \rangle = 0.098(0.052)$, $\langle \hat{S}_{\ell}^z \hat{S}_m^z \rangle = -0.020$,

for X -bond(Y -bond).

Comparison with experiments.— Our effective spin model reproduces not only the zigzag order but magnetic specific heat and anisotropic uniform magnetic susceptibilities consistently with experiments, as shown in Fig. 2(b) and (c). For the specific heat, our results are consistent without adjustable parameters. The uniform magnetic susceptibilities χ show Curie-Weiss behaviors and $\chi_{ab} < \chi_c$, where χ_{ab} (χ_c) is the inplane (out-of-plane) susceptibility, which are consistent with experiments. If we introduce a g -factor, $g = 1.5$, and anisotropic van Vleck term, $\chi_0 = 1 \times 10^{-4} \text{ cm}^3/\text{mol}$ for χ_c , high-temperature behaviors of χ are qualitatively reproduced as shown in Fig. 2(c). Here we note that the electron's spin moments are different from those of the effective spin models depending on the choice of the Kramers doublets, $|\uparrow\rangle$ and $|\downarrow\rangle$ (see Appendix C). For the calculation of χ , we project the original Zeeman term to the effective spin basis $\hat{S}_\ell^{x,y,z}$ (see Eq.(11) in Appendix C). It is left for future studies to relate linear spin wave analysis of our model to the inelastic neutron scattering experiment [7].

Phase diagram in lattices distorted from Na_2IrO_3 .— Now we examine the sensitivity of the ground state for the *ab initio* parameter of Na_2IrO_3 to perturbations and search candidates of other quantum states possibly induced by a thermodynamic control such as pressure or in derivatives of Na_2IrO_3 such as $\text{Na}_{2-x}\text{Li}_x\text{IrO}_3$ [28]. Here we choose the trigonal distortion Δ as an experimentally accessible control parameter. First, the Δ -dependence of the exchange couplings is illustrated in Fig.3(a), where the parameters of the *ab initio* t_{2g} -hamiltonian other than Δ are kept unchanged, and the exchange couplings are estimated from the same strong coupling expansion by changing Δ . The ground state of the generalized Kitaev-Heisenberg model with the Δ -dependent exchange couplings is shown in Fig.3(b).

How to approach spin liquids.— As already evident in Table.II, the *ab initio* effective spin model for Na_2IrO_3 is governed by dominant Kitaev-type ferromagnetic exchange couplings. By expanding the lattice, the spin liquid phase may become accessible: Expansion of the lattice makes the hopping parameters other than the dominant one t negligible. In addition, the environment of the iridium atoms approach the spherical limit where the intra-orbital Coulomb repulsion U' satisfies $U' = U - 2J_H$. Indeed, when we omit the hopping parameters other than t and increase J_H up to 0.3 eV to satisfy $U' = U - 2J_H$, we obtain the spin liquid states adiabatically connected to the Kitaev's spin liquid as shown in Fig. 3(c).

Summary.— We have shown that the realistic parameter of the *ab initio* model for Na_2IrO_3 reproduces the experimentally observed robust zigzag magnetic order, while a quantum spin liquid phase adiabatically connected to the Kitaev spin liquid emerges when the smaller

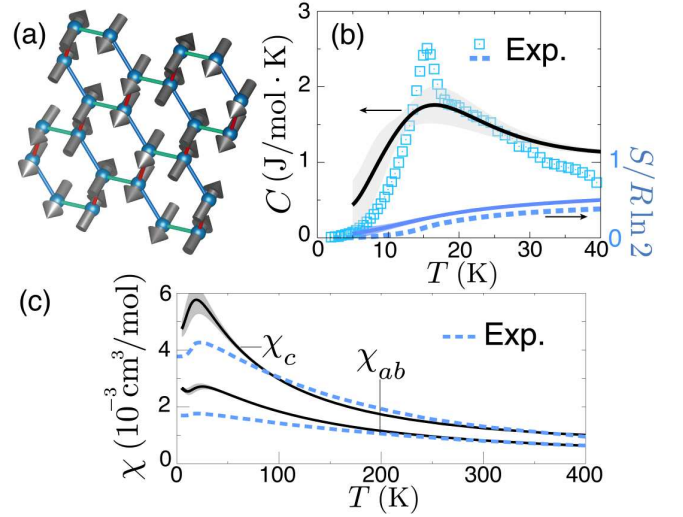


FIG. 2: (color online): Ground state and finite temperature properties of the generalized Kitaev-Heisenberg model for Na_2IrO_3 calculated for the 24-site cluster by using the Lanczos method and thermal pure quantum states [24]. (a) Ground state magnetic order determined by applying tiny local magnetic fields ($\sim 10^{-2}$ meV) at a single site. (b) Temperature-dependence of specific heat C and entropy S , which are consistent with an experiment [29]. Shaded area shows uncertainty due to finite size effects [24]. (c) Temperature-dependence of inplane and out-of-plane magnetic susceptibilities, which are also consistent with the experiment [29] at high temperatures.

trigonal distortion Δ and expanded lattice constants are satisfied. In this sense, uniaxial strain to reduce Δ is helpful as an approach to realize the spin liquids. Clearly further studies are needed: More accurate estimate of the phase diagram of the generalized Kitaev-Heisenberg model is certainly helpful. More detailed studies by taking account of full quantum fluctuations and the effects of realistic itinerancy beyond the strong coupling limit are future intriguing issues.

The authors thank Tsuyoshi Okubo for sharing his unpublished data. Y. N. is supported by the Grant-in-Aid for JSPS Fellows (Grant No.12J08652). M. K. is supported by Grant-in-Aid for JSPS Fellows (Grant No.12J07338). R. A. is supported by Funding Program for World-Leading Innovative R&D on Science and Technology (FIRST program) on “Quantum Science on Strong Correlation.” This work is financially supported by MEXT HPCI Strategic Programs for Innovative Research (SPIRE) (hp130007) and Computational Materials Science Initiative (CMSI). Numerical calculation was partly carried out at the Supercomputer Center, Institute for Solid State Physics, Univ. of Tokyo. This work was also supported by Grant-in-Aid for Scientific Research (No. 22104010, and No. 223400901) from MEXT, Japan.

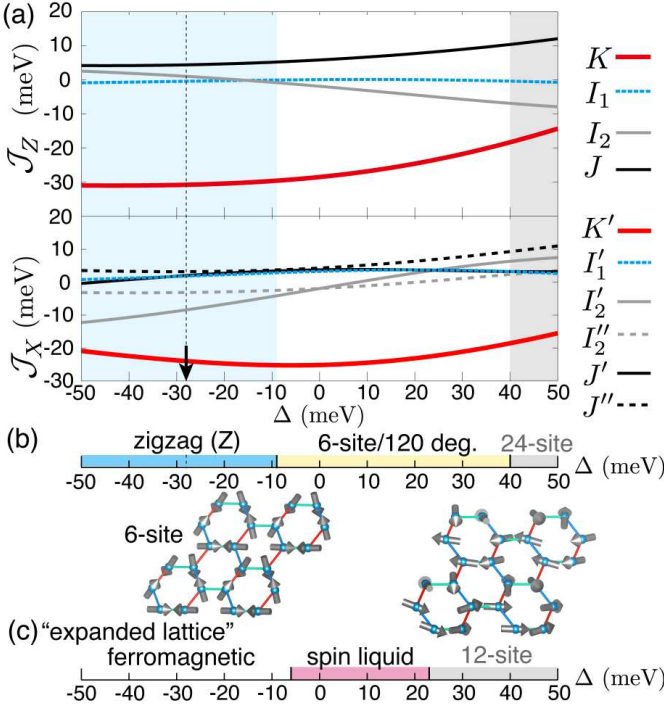


FIG. 3: (color online): (a) Δ -dependence of matrix elements of \mathcal{J}_Z , \mathcal{J}_X as functions of Δ . Around the *ab initio* values at Δ (~ -28 meV) listed in Table II, $K < 0$, $K' < 0$, $J > 0$, $J' > 0$, and $J'' > 0$ are stably satisfied with gradual dependences on Δ . (b) Ground state phase diagram for Na_2IrO_3 with lattice distortions represented by changes in Δ . The phase boundaries are determined by anomalies (peaks signaling continuous transitions) in second derivatives of the exact energy for the 24-site cluster with respect to Δ . Around the *ab initio* parameter $\Delta = -28$ meV, the zigzag order appears. By increasing Δ , a 6-site unit cell order (or 120°-structure [27]) illustrated in the lower left panel and a 24-site unit cell long-period order (see Appendix H), appear. (c) Δ -dependence of the ground state of the generalized Kitaev-Heisenberg model for “expanded lattices.” Here we neglect the small hopping parameters other than t and take a larger Hund’s rule coupling $J_H = 0.3$ eV. Spin liquid phases compete with ferromagnetic states and 12-site unit cell orders illustrated in the upper right panel (see Appendix H), where the phase transitions among them are also interpreted as continuous ones.

Appendix A: Details of DFT electronic structure

The global electronic structure was obtained by performing the density functional calculations using the Elk full-potential linearized augmented plane-wave code with the Perdew-Wang exchange-correlation functional. (See Refs.17 and 18.) The muffin tin radii (R_{MT}) of 1.61, 2.14, and 1.55 bohr for Na, Ir and O were used, respectively. The maximum modulus for the reciprocal vectors K_{max} was chosen such that $R_{\text{MT}}^{\text{min}} K_{\text{max}} = 7.0$, where $R_{\text{MT}}^{\text{min}}$ is the smallest R_{MT} in the system.

The present DFT calculation agrees with previously reported results. Here we show the density of states

(DOS) in Fig. 4, which is consistent with DOS reported in Ref.15 of the main article.

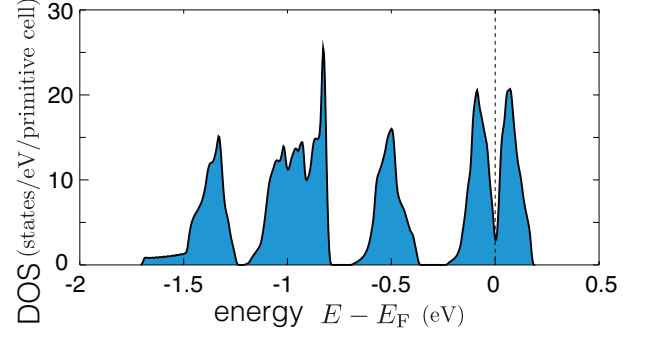


FIG. 4: Density of states (DOS) of Na_2IrO_3 calculated by using the Elk full-potential linearized augmented plane-wave code (see the main article and Ref.15). The crystal structure with the $C2/m$ (No.12) space group is used, where two iridium atoms exist in the primitive cell.

For the calculation of the partially screened Coulomb interaction, we took 100 unoccupied bands and $4 \times 4 \times 3$ \mathbf{k} and \mathbf{q} meshes, and the double Fourier transform of constrained susceptibility χ_0 was done with the cutoff of $|\mathbf{G} + \mathbf{q}| = 5$ (1/a.u.) with \mathbf{G} being the reciprocal vector.

Appendix B: Ground state of local hamiltonian

The eigenstates of the t_{2g} -shell of an isolated iridium ion Ir^{+4} is described by the local hamiltonian $\hat{H}_{\text{tri}} + \hat{H}_{\text{SOC}} + \hat{H}_U$. For any amplitude of the trigonal distortion Δ , the atomic ground state with 5 electrons in the t_{2g} -shell is a doublet, as shown in Fig. 5. The excitation gap among the ground state doublet and the excited doublet is always larger than $\zeta_{\text{so}} = 0.39$ eV. Here, we note that, due to the orbital-dependent chemical potentials μ_a ($a = xy, yz, zx$), even for $\Delta = 0$, there is the finite energy gap between the first and second excited states. Therefore, the present pseudo-spin model derived in the main article remains valid at temperatures roughly lower than $\zeta_{\text{so}}/k_B \simeq 4 \times 10^3$ K.

Appendix C: Relationship between physical and effective spins

Due to the trigonal distortion, $\text{SU}(2)$ rotation and $\text{U}(1)$ gauge transformation of electron wave functions for the Kramers doublet change the matrix elements of \mathcal{J}_T ($T = X, Y, Z$), \mathcal{J}_2 , and \mathcal{J}_3 , where, for further neighbor exchange couplings \mathcal{J}_2 , and \mathcal{J}_3 , details are given in the following Appendix D. In the present Letter, we choose a Kramers doublet $|\uparrow\rangle$ and $|\downarrow\rangle$ as

$$|\uparrow\rangle = z_1 \hat{c}_{yz\downarrow}^\dagger \hat{c}_{zx\uparrow}^\dagger \hat{c}_{zx\downarrow}^\dagger \hat{c}_{xy\uparrow}^\dagger \hat{c}_{xy\downarrow}^\dagger |0\rangle$$

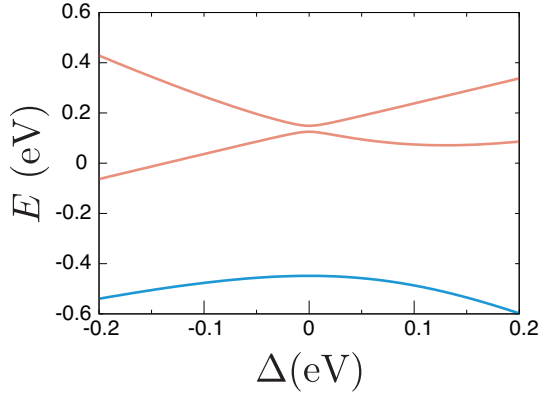


FIG. 5: Three doublet eigenstates of the local hamiltonian $\hat{H}_{\text{tri}} + \hat{H}_{\text{SOC}}$ with 5 electrons in the t_{2g} -shell as functions of the trigonal distortion Δ . The Coulomb term \hat{H}_U causes a constant shift in these three doublets. The doublet ground state is shown in the blue curve, while the red curves represent the excited doublet states.

$$\begin{aligned}
 & + z_2 \hat{c}_{yz\uparrow}^\dagger \hat{c}_{zx\uparrow}^\dagger \hat{c}_{zx\downarrow}^\dagger \hat{c}_{xy\uparrow}^\dagger \hat{c}_{xy\downarrow}^\dagger |0\rangle \\
 & + z_1^* \hat{c}_{yz\uparrow}^\dagger \hat{c}_{yz\downarrow}^\dagger \hat{c}_{zx\downarrow}^\dagger \hat{c}_{xy\uparrow}^\dagger \hat{c}_{xy\downarrow}^\dagger |0\rangle \\
 & - iz_2 \hat{c}_{yz\uparrow}^\dagger \hat{c}_{yz\downarrow}^\dagger \hat{c}_{zx\uparrow}^\dagger \hat{c}_{xy\uparrow}^\dagger \hat{c}_{xy\downarrow}^\dagger |0\rangle \\
 & - h \hat{c}_{yz\uparrow}^\dagger \hat{c}_{yz\downarrow}^\dagger \hat{c}_{zx\uparrow}^\dagger \hat{c}_{zx\downarrow}^\dagger \hat{c}_{xy\downarrow}^\dagger |0\rangle \\
 & + e^{-i\pi/4} f \hat{c}_{yz\uparrow}^\dagger \hat{c}_{yz\downarrow}^\dagger \hat{c}_{zx\uparrow}^\dagger \hat{c}_{zx\downarrow}^\dagger \hat{c}_{xy\uparrow}^\dagger |0\rangle, \quad (9)
 \end{aligned}$$

and

$$\begin{aligned}
 |\downarrow\rangle & = -z_2^* \hat{c}_{yz\downarrow}^\dagger \hat{c}_{zx\uparrow}^\dagger \hat{c}_{zx\downarrow}^\dagger \hat{c}_{xy\uparrow}^\dagger \hat{c}_{xy\downarrow}^\dagger |0\rangle \\
 & + z_1^* \hat{c}_{yz\uparrow}^\dagger \hat{c}_{zx\uparrow}^\dagger \hat{c}_{zx\downarrow}^\dagger \hat{c}_{xy\uparrow}^\dagger \hat{c}_{xy\downarrow}^\dagger |0\rangle \\
 & - iz_2^* \hat{c}_{yz\uparrow}^\dagger \hat{c}_{yz\downarrow}^\dagger \hat{c}_{zx\downarrow}^\dagger \hat{c}_{xy\uparrow}^\dagger \hat{c}_{xy\downarrow}^\dagger |0\rangle \\
 & + z_1 \hat{c}_{yz\uparrow}^\dagger \hat{c}_{yz\downarrow}^\dagger \hat{c}_{zx\uparrow}^\dagger \hat{c}_{xy\uparrow}^\dagger \hat{c}_{xy\downarrow}^\dagger |0\rangle \\
 & - e^{+i\pi/4} f \hat{c}_{yz\uparrow}^\dagger \hat{c}_{yz\downarrow}^\dagger \hat{c}_{zx\uparrow}^\dagger \hat{c}_{zx\downarrow}^\dagger \hat{c}_{xy\downarrow}^\dagger |0\rangle \\
 & - h \hat{c}_{yz\uparrow}^\dagger \hat{c}_{yz\downarrow}^\dagger \hat{c}_{zx\uparrow}^\dagger \hat{c}_{zx\downarrow}^\dagger \hat{c}_{xy\uparrow}^\dagger |0\rangle, \quad (10)
 \end{aligned}$$

where z_1 , z_2 , f and h are coefficients of the linear combinations. In the above parameterization of the Kramers doublets, the $J_{\text{eff}} = 1/2$ -state is represented by taking the coefficients $z_1 = (1-i)/\sqrt{6}$, $z_2 = h = 0$, and $f = 1/\sqrt{6}$. Our choice for the above Kramers doublet give us real number elements in the nearest-neighbor exchange coupling along the Z -bond, \mathcal{J}_Z .

For the *ab initio* model, we choose the parameter set (z_1, z_2, f, h) that diagonalizes the z -component of the reduced spin operators for the t_{2g} -manifold defined as

$$\left[\tilde{S}_{\text{tot}}^\alpha \right]_{\sigma\sigma'} = \langle \sigma | \sum_a \sum_{\sigma'} \hat{c}_{a\sigma}^\dagger \hat{\sigma}^\alpha \hat{c}_{a\sigma'} / 2 | \sigma' \rangle, \quad (11)$$

where $\alpha = x, y, z$. By using the resultant Kramers doublet, the total magnetic moment consisting of the reduced spin and angular momentum operators, $\tilde{S}_{\text{tot}}^\alpha$ and $\tilde{L}_{\text{tot}}^\alpha$, for

the t_{2g} -manifold is expressed by the $\text{SU}(2)$ operators \hat{S}^α . For the *ab initio* model, the total magnetic moment is given as

$$\begin{bmatrix} 2\tilde{S}_{\text{tot}}^x - \tilde{L}_{\text{tot}}^x \\ 2\tilde{S}_{\text{tot}}^y - \tilde{L}_{\text{tot}}^y \\ 2\tilde{S}_{\text{tot}}^z - \tilde{L}_{\text{tot}}^z \end{bmatrix} = 2 \begin{bmatrix} -0.07 & +0.94 & -0.24 \\ +0.94 & -0.07 & +0.24 \\ -0.07 & +0.07 & +1.07 \end{bmatrix} \begin{bmatrix} \hat{S}^x \\ \hat{S}^y \\ \hat{S}^z \end{bmatrix}. \quad (12)$$

For the calculation of the uniform magnetic susceptibilities χ , we reduce the original Zeeman term,

$$-\mu_B (2\tilde{S} - \tilde{L}) \cdot \vec{B},$$

to the effective spin basis $\hat{S}_\ell^{x,y,z}$ through Eq.(12).

Appendix D: Further neighbor exchange couplings and details of the hopping parameters

For quantitative accuracy, we include dominant 2nd and 3rd neighbor exchange couplings represented by \hat{H}' for our numerical calculations:

$$\hat{H}' = \sum_{\langle \ell, m \rangle' \in Z_{2nd}} \vec{S}_\ell^T \mathcal{J}_2 \vec{S}_m + \sum_{\langle \ell, m \rangle''} \vec{S}_\ell^T \mathcal{J}_3 \vec{S}_m, \quad (13)$$

where further exchange couplings are given in matrices \mathcal{J}_2 , and \mathcal{J}_3 . The summations are over the second neighbor pairs $\langle \ell, m \rangle'$, and the third neighbor pairs $\langle \ell, m \rangle''$. For the 2nd neighbor pairs, exchange couplings are finite if they belong to the group of 2nd neighbor bonds perpendicular to the Z -bond, Z_{2nd} . These exchange matrices are parametrized as

$$\mathcal{J}_2 = \begin{bmatrix} J^{(2nd)} & I_1^{(2nd)} & I_2^{(2nd)} \\ I_1^{(2nd)} & J^{(2nd)} & I_2^{(2nd)} \\ I_2^{(2nd)} & I_2^{(2nd)} & K^{(2nd)} \end{bmatrix}, \quad (14)$$

and

$$\mathcal{J}_3 = \begin{bmatrix} J^{(3rd)} & 0 & 0 \\ 0 & J^{(3rd)} & 0 \\ 0 & 0 & J^{(3rd)} \end{bmatrix}, \quad (15)$$

where the obtained parameters are given in Table III. The all of the matrix elements of the 2nd and 3rd neighbor exchange couplings for other bonds, Dzyaloshinskii-Moriya-type couplings, as well as the couplings for even further neighbor bonds are smaller than 1 meV and neglected.

For derivation of these exchange parameters, we use detailed *ab initio* hopping parameters summarized in Table IV.

\mathcal{J}_2 (meV)	$K^{(2nd)}$	$J^{(2nd)}$	$I_1^{(2nd)}$	$I_2^{(2nd)}$
	-1.2	-0.8	1.0	-1.4
\mathcal{J}_3 (meV)	$J^{(3rd)}$			
	1.7			

TABLE III: Second and third neighbor exchange couplings derived by the strong coupling expansion from the *ab initio* t_{2g} model.

Z	$yz \uparrow$	$yz \downarrow$	$zx \uparrow$	$zx \downarrow$	$xy \uparrow$	$xy \downarrow$
$yz \uparrow$	31+0i	0+0i	273+8i	4+4i	-16-2i	10+39i
$yz \downarrow$	0+0i	31+0i	-4+4i	273-8i	-10+39i	-16+2i
$zx \uparrow$	273-8i	-4-4i	31+0i	0+0i	-16+2i	-39-10i
$zx \downarrow$	4-4i	273+8i	0+0i	31+0i	39-10i	-16-2i
$xy \uparrow$	-16+2i	-10-39i	-16-2i	39+10i	43+0i	0+0i
$xy \downarrow$	10-39i	-16-2i	-39+10i	-16+2i	0+0i	43+0i
X	$yz \uparrow$	$yz \downarrow$	$zx \uparrow$	$zx \downarrow$	$xy \uparrow$	$xy \downarrow$
$yz \uparrow$	-7+0i	0+0i	-18-11i	-36+3i	-25+39i	11-2i
$yz \downarrow$	0+0i	-7+0i	36+3i	-18+11i	-11-2i	-25-39i
$zx \uparrow$	-18+11i	36-3i	36+0i	0+0i	276+5i	5+8i
$zx \downarrow$	-36-3i	-18-11i	0+0i	36+0i	-5+8i	276-5i
$xy \uparrow$	-25-39i	-11+2i	276-5i	-5-8i	38+0i	0+0i
$xy \downarrow$	11+2i	-25+39i	5-8i	276+5i	0+0i	38+0i
Z_{2nd}	$yz \uparrow$	$yz \downarrow$	$zx \uparrow$	$zx \downarrow$	$xy \uparrow$	$xy \downarrow$
$yz \uparrow$	0-3i	0+4i	-85+0i	-2-2i	12-2i	-1+9i
$yz \downarrow$	0+4i	0+3i	2-2i	-85+0i	1+9i	12+2i
$zx \uparrow$	-30+1i	-2-2i	0-3i	4+0i	-20+3i	-10+0i
$zx \downarrow$	2-2i	-30-1i	-4+0i	0+3i	10+0i	-20-3i
$xy \uparrow$	-20+3i	0-10i	12-2i	9-1i	-2+6i	0+0i
$xy \downarrow$	0-10i	-20-3i	-9-1i	12+2i	0+0i	-2-6i
Z_{3rd}	$yz \uparrow$	$yz \downarrow$	$zx \uparrow$	$zx \downarrow$	$xy \uparrow$	$xy \downarrow$
$yz \uparrow$	-10+0i	0+0i	-13+0i	-1-1i	18+0i	0+4i
$yz \downarrow$	0+0i	-10+0i	1-1i	-13+0i	0+4i	18+0i
$zx \uparrow$	-13+0i	1+1i	-10+0i	0+0i	18+0i	-4+0i
$zx \downarrow$	-1+1i	-13+0i	0+0i	-10+0i	4+0i	18+0i
$xy \uparrow$	18+0i	0-4i	18+0i	4+0i	-37+0i	0+0i
$xy \downarrow$	0-4i	18+0i	-4+0i	18+0i	0+0i	-37+0i

TABLE IV: Detailed hopping parameters for nearest-, 2nd, and 3rd neighbor pairs of the iridium sites. The unit of the hopping parameters is given by meV. For the nearest-neighbor hoppings, the hoppings along the Z -bond and X -bond are shown, where the hoppings along the Y -bond is obtained by exchanging indices in the hoppings along the X -bond. The directions of these hopping processes are illustrated in Fig. 8(a) later.

Appendix E: Second order perturbation

In the present Letter, we derive a generalized Kitaev-Heisenberg model by employing second-order degenerated perturbation theory from a strong coupling limit: We perform the perturbation by taking $\hat{H}_{\text{tri}} + \hat{H}_{\text{SOC}} + \hat{H}_U$ as the unperturbed hamiltonian and \hat{H}_0 as the perturbation.

As clarified in the Appendix D, the ground state of the local part of the unperturbed hamiltonian $\hat{H}_{\text{tri}} + \hat{H}_{\text{SOC}} +$

\hat{H}_U is a Kramers doublet, but, strictly speaking, it deviates from the so-called $J_{\text{eff}} = 1/2$ state if $\Delta \neq 0$. We assign pseudo-spin degree of freedom to this doublet.

For illustrative purpose, we focus on a set of nearest-neighbor sites, the ℓ -th and m -th sites. Then we calculate the perturbation energy through the second order processes as

$$E_{\sigma_1, \sigma_2; \sigma_3, \sigma_4}^{(2)} = \langle m\sigma_2 | \langle \ell\sigma_1 | \hat{H}_0 \sum_n \frac{|n\rangle\langle n|}{E_n - E_0} \hat{H}_0 | \ell\sigma_3 \rangle | m\sigma_4 \rangle, \quad (16)$$

where $\sigma_j = \uparrow, \downarrow$ ($j = 1, 2, 3, 4$) is a pseudo-spin index, and $|n\rangle$ is an intermediate eigenstate of $\hat{H}_{\text{tri}} + \hat{H}_{\text{SOC}} + \hat{H}_U$ with 4 and 6 electrons at the ℓ -th and m -th site, respectively, or 6 and 4 electrons at the ℓ -th and m -th site, respectively. Here E_0 is the ground-state energy of the two sites with 5 electrons per site and E_n is an energy eigenvalues of an intermediate state of the two sites. The eigenstates $|n\rangle$ and eigenvalues E_n are obtained by numerically diagonalizing $\hat{H}_{\text{tri}} + \hat{H}_{\text{SOC}} + \hat{H}_U$.

From the perturbation energy $E_{\sigma_1, \sigma_2; \sigma_3, \sigma_4}^{(2)}$, we obtain the exchange couplings as follows. If we assume the bond connecting the ℓ -th and m -th sites is a Z -bond, the exchange couplings are given for the minimal spin model for $A_2\text{IrO}_3$ as

$$K = +2 \left[E_{\sigma, \sigma; \sigma, \sigma}^{(2)} - E_{\sigma, \bar{\sigma}; \sigma, \bar{\sigma}}^{(2)} \right], \quad (17)$$

$$J = +2 E_{\sigma, \bar{\sigma}; \bar{\sigma}, \sigma}^{(2)}, \quad (18)$$

$$I_1 = -2 \text{Im} \left\{ E_{\uparrow, \uparrow; \downarrow, \downarrow}^{(2)} \right\} = +2 \text{Im} \left\{ E_{\downarrow, \downarrow; \uparrow, \uparrow}^{(2)} \right\}, \quad (19)$$

$$\begin{aligned} I_2 &= +4 \text{Re} \left\{ E_{\uparrow, \uparrow; \uparrow, \downarrow}^{(2)} \right\} = -4 \text{Im} \left\{ E_{\uparrow, \uparrow; \downarrow, \downarrow}^{(2)} \right\} \\ &= +4 \text{Re} \left\{ E_{\uparrow, \uparrow; \downarrow, \uparrow}^{(2)} \right\} = -4 \text{Im} \left\{ E_{\uparrow, \uparrow; \uparrow, \uparrow}^{(2)} \right\} \\ &= -4 \text{Re} \left\{ E_{\downarrow, \downarrow; \downarrow, \downarrow}^{(2)} \right\} = -4 \text{Im} \left\{ E_{\downarrow, \downarrow; \uparrow, \downarrow}^{(2)} \right\} \\ &= -4 \text{Re} \left\{ E_{\downarrow, \downarrow; \uparrow, \uparrow}^{(2)} \right\} = -4 \text{Im} \left\{ E_{\downarrow, \downarrow; \downarrow, \uparrow}^{(2)} \right\}. \end{aligned} \quad (20)$$

For the 2nd and 3rd neighbor bond, the matrix elements of the exchange couplings \mathcal{J}_2 and \mathcal{J}_3 as functions of the trigonal distortion Δ are calculated by the 2nd order perturbation as shown in Fig. 6.

Appendix F: An estimate of contributions from e_g -orbitals

In Ref.11, it was proposed that the t_{2g} - e_g hoppings might play an important role in determining the signs of the Kitaev couplings. However, we show that they give only small corrections to the Kitaev couplings, K and K' by employing the estimation of Ref.11 combined with parameters expected from our *ab initio* parameters for the t_{2g} -manifold. Following Ref.11, we employ the formula, $(4/9)(\tilde{t}/\tilde{U})^2 \tilde{J}_H$ for the contribution of the t_{2g} - e_g

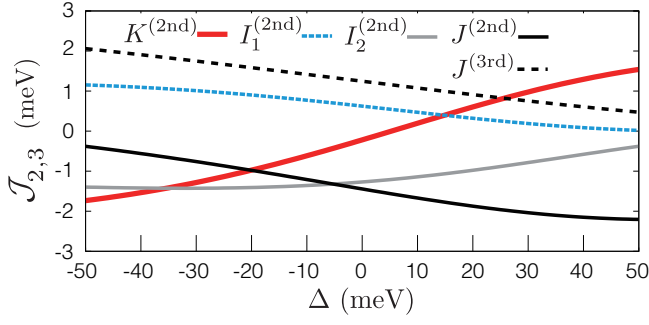


FIG. 6: Exchange couplings for 2nd and 3rd neighbor bond as functions of Δ .

hoppings to the Kitaev couplings. To evaluate the formula, we choose the t_{2g-e_g} hoppings $\tilde{t} = 2t = 0.54$ eV, the Hund's rule coupling among the t_{2g} - and e_g -orbitals, $\tilde{J}_H = J_H = 0.23$ eV, and the excitation energy of intermediate states for the 2nd order perturbation process, $\tilde{U} = U - V + \Delta_{e_g t_{2g}} = 2.7 - 1.1 + 3 = 4.6$ eV, where the crystal field splitting between the e_g and t_{2g} , $\Delta_{e_g t_{2g}} = 3$ eV, is estimated from the *ab initio* band structure given in Ref.15. Then, the correction to the Kitaev coupling from the $t_{2g}-e_g$ hoppings is estimated as $(4/9)(\tilde{t}/\tilde{U})^2 \tilde{J}_H = 1.4$ meV, which is less than 6 percent of our *ab initio* estimate of K and K' . Therefore, the $t_{2g}-e_g$ hoppings introduce minor quantitative corrections and do not change the sign of the Kitaev couplings, which justifies our t_{2g} hamiltonian as a proper effective low-energy hamiltonian.

Appendix G: Stabilization of zigzag magnetic orders

As explained in the main article, the zigzag order found as the ground state of the *ab initio* model is interpreted as antiferromagnetically coupled ferromagnetic chains, which is stabilized by the three exchange couplings, $K \sim K' < 0$, $J > 0$, and $I_2'' < 0$. As explained later, another exchange coupling I_2' , which seemingly dominates I_2'' , is irrelevant to the zigzag (Z) order. To demonstrate this, we show that the zigzag order which is adiabatically connected to that of the *ab initio* model is indeed realized in a simplified model with these three exchange couplings, $K \sim K' < 0$, $J > 0$, and $I_2'' < 0$, defined as

$$\hat{H}_{KJI_2''} = \sum_{\Gamma=X,Y,Z} \sum_{\langle \ell, m \rangle \in \Gamma} \vec{S}_\ell^T \mathcal{J}_\Gamma^{(0)} \vec{S}_m, \quad (21)$$

where the matrices of the exchange couplings are given by

$$\mathcal{J}_Z^{(0)} = \begin{bmatrix} J & 0 & 0 \\ 0 & J & 0 \\ 0 & 0 & K \end{bmatrix}, \mathcal{J}_X^{(0)} = \begin{bmatrix} K & I_2'' & 0 \\ I_2'' & 0 & 0 \\ 0 & 0 & 0 \end{bmatrix},$$

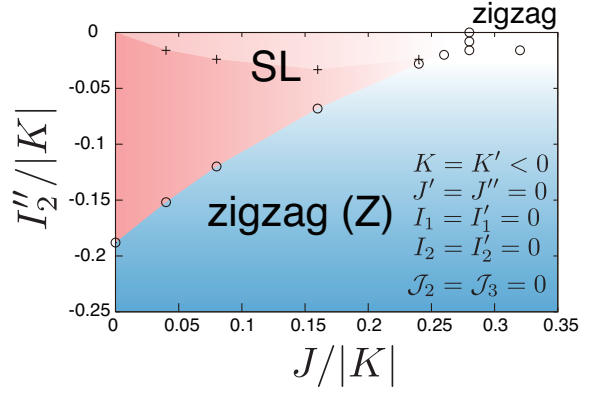


FIG. 7: Phase diagram for the ground states of the simplified model, $\hat{H}_{KJI_2''}$, with $K = K' < 0$, $J > 0$, and $I_2'' < 0$, defined in Eqs. (21) and (22). There are mainly two kind of phases: spin liquid (SL) phases adiabatically connected to the Kitaev limit ($J = I_2'' = 0$) (red region) and zigzag order phases (blue region). Especially, the phase denoted as zigzag (Z) shows the Bragg peak located at the momentum $(0, 1)$ shown as blue diamonds in Fig. 8(b). For small amplitude of I_2'' and $J/|K| > 0.28$, zigzag-type magnetic correlations are enhanced but are accompanied with additional peaks as well corresponding to other alignments of zigzag orders, which makes a clear determination of the phase difficult. For determination of other phase boundaries, the second derivatives of the ground state energy with respect to J or I_2'' are employed. To identify the phase without ambiguity, we also check the calculated results on Bragg peaks in the magnetic structure factors. Open circles indicate continuous phase transitions (or peaks in the second derivatives of the ground state energy), and crosses indicate first order phase transitions (or cusps (level crossings) in the ground state energy).

$$\mathcal{J}_Y^{(0)} = \begin{bmatrix} 0 & I_2'' & 0 \\ I_2'' & K & 0 \\ 0 & 0 & 0 \end{bmatrix}. \quad (22)$$

The ground states of the simplified model $\hat{H}_{KJI_2''}$ are summarized as the phase diagram in Fig. 7. The three exchange couplings, $K \sim K' < 0$, $J > 0$, and $I_2'' < 0$, indeed stabilize the zigzag order, and the positions of the Bragg peaks are identical with those of the zigzag-ordered phase obtained by the *ab initio* model, which is denoted as zigzag (Z) in Fig. 8. We have confirmed that the present zigzag ordered phase is adiabatically connected with the zigzag order found in the *ab initio* model.

Here we note that the present model with the three exchange couplings, K , I_2'' , and J , is given by straightforward simplification of the *ab initio* model: First, we discard small exchange couplings, I_1 , I_2 , J , I_1' , J_2 , and J_3 , with amplitudes less than 3 meV. Then, we drop the sub-dominant Heisenberg term J'' . As explained below, I_2' is irrelevant for the zigzag (Z) order and, therefore, is dropped in the present three-exchange-coupling model.

By averaging the *ab initio* Kitaev couplings as $(K + 2K')/3 \sim 26$ meV, the parameter set $I_2''/|K| = -0.12$

and $J/|K| = 0.17$ corresponds to the *ab initio* model and gives the zigzag (Z) order as shown in Fig. 7. For the parameter set, when we introduce additional I'_2 up to $I'_2/|K| = -0.32$ that corresponds to the *ab initio* value, we confirm that the ground state remains the zigzag (Z) order for the 24-site cluster.

We also note that, in the simplified three-exchange-coupling model, the difference between $\mathcal{J}_Z^{(0)}$ and $\mathcal{J}_X^{(0)}$ (or $\mathcal{J}_Y^{(0)}$) inherits from the anisotropic crystal structure that differentiates Ir-Ir bonds along the b -axis from other bonds. If we take an isotropic exchange couplings for $\mathcal{J}_Z^{(0)}$, $\mathcal{J}_X^{(0)}$, and $\mathcal{J}_Y^{(0)}$, we do not obtain the zigzag (Z) states as the ground states, which indicates that the inherent anisotropy plays an important role in realizing the zigzag (Z) order.

Appendix H: Magnetic Bragg peaks and pinning field analysis

zigzag (Z)	6-site/120°	24-site	12-site
(0, 1)	(1/3, 1)	(1/6, 1/2)	(1/3, 0)

TABLE V: List of the momenta at which the dominant peaks appear in the magnetic structure factors calculated for each magnetic ordered phases in the phase diagrams, Fig. 3(b) and (c) of the main article. Momenta are defined in a two dimensional Brillouin zone that is used in Ref.7 of the main article and Fig. 8.

Peaks in spin structure factors, which may correspond to the magnetic Bragg peaks in the thermodynamic limit, are primarily used to determine magnetic orders in the exact diagonalization. The 2D unit cell in the honeycomb layer of Na_2IrO_3 and the peaks of the spin structure factors are shown in Fig. 8. In Table V, the magnetic Bragg peak positions in the two-dimensional Brillouin zone are summarized.

However, anisotropy in alignments of ordered moments cannot be determined by the magnetic Bragg spots. Therefore we applied tiny local magnetic fields ($\sim 10^{-2}$ meV) to break symmetries and pin down the magnetic order pattern during the Lanczos steps. In Fig. 2 and Fig. 3 of the main article, normalized induced moments are illustrated.

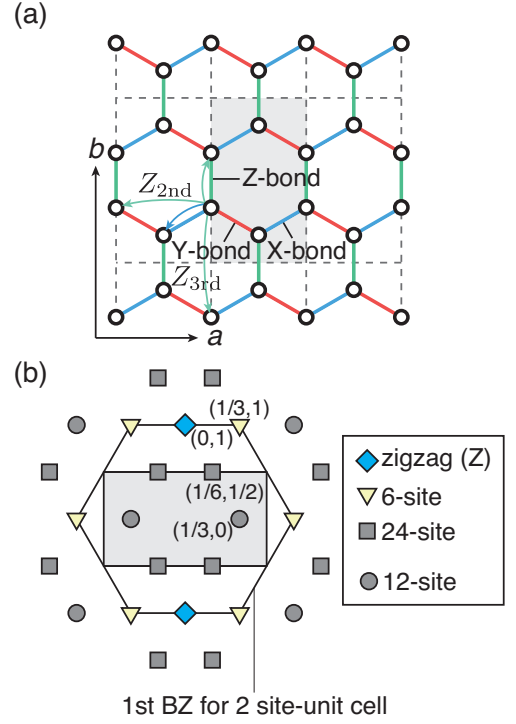


FIG. 8: (a) Experimental unit cell for honeycomb planes of iridium atoms. The horizontal and vertical axes represent the a - and b -axis of Na_2IrO_3 . The shaded rectangular area illustrates an unit cell consisting of 4 iridium atoms. The arrows illustrate the direction of the hoppings summarized in Table IV. (b) Peaks in spin structure factors calculated by using the Lanczos method for the 24-site cluster. The shaded rectangular area illustrates the 1st Brillouin zone (BZ) of Na_2IrO_3 . The hexagon represents the 1st Brillouin zone of the ideal honeycomb lattice whose unit cell contains two sites.

[1] G. Jackeli and G. Khaliullin, Phys. Rev. Lett. **102**, 017205 (2009).
[2] J. Chaloupka, G. Jackeli, and G. Khaliullin, Phys. Rev. Lett. **105**, 027204 (2010).
[3] X. Wan, A. M. Turner, A. Vishwanath, and S. Y. Savrasov, Phys. Rev. B **83**, 205101 (2011).

[4] W. Witczak-Krempa, C. Gang, Y.-B. Kim, and L. Balents, arXiv:1305.2193.
[5] A. Kitaev, Annals Phys. **321**, 2 (2006).
[6] R. Comin, G. Levy, B. Ludbrook, Z.-H. Zhu, C. Veenstra, J. Rosen, Y. Singh, P. Gegenwart, D. Stricker, J. Hancock, et al., Phys. Rev. Lett. **109**, 266406 (2012).
[7] S. K. Choi, R. Coldea, A. N. Kolmogorov, T. Lancaster, I. I. Mazin, S. J. Blundell, P. G. Radaelli, Y. Singh, P. Gegenwart, K. R. Choi, et al., Phys. Rev. Lett. **108**, 127204 (2012).
[8] F. Ye, S. Chi, H. Cao, B. C. Chakoumakos, J. A. Fernandez-Baca, R. Custelcean, T. F. Qi, O. B. Korneta, and G. Cao, Phys. Rev. B **85**, 180403 (2012).
[9] Y. Singh, S. Manni, J. Reuther, T. Berlijn, R. Thomale, W. Ku, S. Trebst, and P. Gegenwart, Phys. Rev. Lett. **108**, 127203 (2012).
[10] J. Reuther, R. Thomale, and S. Trebst, Phys. Rev. B **84**, 100406 (2011).
[11] J. Chaloupka, G. Jackeli, and G. Khaliullin, Phys. Rev. Lett. **110**, 097204 (2013).
[12] I. Kimchi and Y.-Z. You, Phys. Rev. B **84**, 180407 (2011).
[13] A. F. Albuquerque, D. Schwandt, B. Hetényi, S. Capponi, M. Mambrini, and A. M. Läuchli, Phys. Rev. B

- 84**, 024406 (2011).
- [14] S. Bhattacharjee, S.-S. Lee, and Y. B. Kim, *New Journal of Physics* **14**, 073015 (2012).
 - [15] I. I. Mazin, H. O. Jeschke, K. Foyevtsova, R. Valentí, and D. I. Khomskii, *Phys. Rev. Lett.* **109**, 197201 (2012).
 - [16] T. Miyake and M. Imada, *J. Phys. Soc. Jpn.* **79**, 112001 (2010).
 - [17] <http://elk.sourceforge.net/>.
 - [18] J. P. Perdew and Y. Wang, *Phys. Rev. B* **45**, 13244 (1992).
 - [19] R. Arita, J. Kuneš, A. V. Kozhevnikov, A. G. Eguiluz, and M. Imada, *Phys. Rev. Lett.* **108**, 086403 (2012).
 - [20] F. Aryasetiawan, M. Imada, A. Georges, K. Gabriel, S. Biermann, and A. I. Lichtenstein, *Phys. Rev. B* **70**, 195104 (2004).
 - [21] A. Kozhevnikov, A. Eguiluz, and T. Schulthess, *SC'10 Proceedings of the 2010 ACM/IEEE International Conference for High Performance Computing, Networking, Storage, and Analysis* p. 1 (2010).
 - [22] V. K. Katukuri, S. Nishimoto, V. Yushankhai, A. Stoyanova, H. Kandpal, C. Sungkyun, R. Coldea, I. Rousochatzakis, L. Hozoi, and J. van den Brink, *New J. Phys.* **16**, 013056 (2014).
 - [23] The small amplitude of the trigonal distortion $\Delta = -28$ meV is different from the previous result[30]. The difference originates from the electronic band structures around the Fermi level in Ref.30 different from the result in Ref.15 and ours. In addition, in Ref.30, the tight-binding parameter is obtained through fitting the LDA dispersion, while we directly calculate the hopping matrix elements with the t_{2g} Wannier orbitals.
 - [24] S. Sugiura and A. Shimizu, *Phys. Rev. Lett.* **108**, 240401 (2012).
 - [25] J. Jaklič and P. Prelovšek, *Phys. Rev. B* **49**, 5065 (1994).
 - [26] M. Imada and M. Takahashi, *J. Phys. Soc. Jpn.* **55**, 3354 (1986).
 - [27] J. G. Rau, E. K.-H. Lee, and H.-Y. Kee, *Phys. Rev. Lett.* **112**, 077204 (2014).
 - [28] G. Cao, T. F. Qi, L. Li, J. Terzic, V. S. Cao, S. J. Yuan, M. Tovar, G. Murthy, and R. K. Kaul, *Phys. Rev. B* **88**, 220414 (2013).
 - [29] Y. Singh and P. Gegenwart, *Phys. Rev. B* **82**, 064412 (2010).
 - [30] C. H. Kim, H. S. Kim, H. Jeong, H. Jin, and J. Yu, *Phys. Rev. Lett.* **108**, 106401 (2012).